International Journal of Energetica (IJECA)
https://www.ijeca.info
ISSN: 2543-3717 Volume 9. Issue 2. 2024 *Page 54-66*

Energy-Efficient Islanding Detection Using CEEMDAN and Neural Network Integration in Photovoltaic Distribution System

Sulayman Kujabi*, Emmanuel Asuming Frimpong, Francis Boafo Effah

Department of Electrical and Electronic Engineering, Kwame Nkrumah University of Science and Technology, Kumasi, GHANA

*Corresponding author E-mail: *kujabisaul@yahoo.com*

Abstract – *This paper proposes an enhanced islanding detection method based on complete ensemble empirical mode decomposition with adaptive noise (CEEMDAN) and a pattern recognition neural network (PANN). Negative sequence voltage data from both islanding and non-islanding scenarios were acquired through MATLAB Simulink simulations, with samples collected at a frequency of 3.84 kHz over a 2.5-second period. The voltage signals were decomposed into intrinsic mode functions (IMFs) using CEEMDAN, after which key features namely normalized max value, standard deviation, and entropy of the IMFs were extracted. The extracted features were used to train the PANN. The model was evaluated using cross-validation and several performance metrics, including accuracy, precision, recall, and F1 score. The proposed model achieved an overall accuracy of 98.6%, with a precision of 100%, a recall of 97%, and an F1 score of 98%. The detection time was found to be 0.2381 seconds, indicating the method's suitability for real-time applications. Furthermore, feature permutation importance analysis highlighted the critical role of certain features in the model's performance. The results demonstrate that the proposed method provides a reliable and efficient solution for islanding detection in grid-connected PV systems, significantly reducing the non-detection zone and ensuring high detection accuracy. This study contributes to developing of advanced detection techniques, enhancing the safety and reliability of modern power systems.*

Keywords: Distributed generation, islanding detection, empirical mode decomposition, pattern artificial neural network, zero non-detection zone, ensemble empirical mode decomposition.

Received: 24/08/2024 – Revised: 05/10/2024 – Accepted: 10/11/2024

I. Introduction

The rapid integration of renewable energy sources, particularly solar photovoltaic (PV) systems, into the power grid has significantly transformed the landscape of modern power systems. While these advancements contribute to sustainable energy solutions, they pose unique challenges to grid stability and reliability. One of the critical issues is the detection of islanding events, where a portion of the grid continues to be powered by distributed generators (DGs) despite disconnection from the main utility grid [1]. Effective islanding detection is essential to ensure the safety of maintenance personnel, protect equipment, and maintain power quality.

Various islanding detection methods have been developed over the years, broadly categorized into passive, active, and hybrid methods. Passive methods rely on monitoring electrical parameters such as voltage, frequency, and harmonic distortion [2]. However, these methods often suffer from larger NDZs and slower detection times, making them less reliable for real-time applications [3].

Active methods introduce perturbations into the system and observe the response to detect islanding events[4]. While these methods can reduce the NDZ, they may adversely affect power quality and require additional

hardware, increasing the overall system complexity and cost [5]. Hybrid methods combine the advantages of both passive and active approaches, aiming to improve detection accuracy and reduce NDZ. However, they still face challenges related to implementation complexity and reliability [6].

Recent signal processing and machine learning advancements have opened new avenues for more effective islanding detection methods.

In [7], the authors proposed feature extraction using Discrete Fourier Transform (DFT) followed by K-nearest neighbour (KNN) classification demonstrating efficient islanding detection. However, relying on DFT for feature extraction may result in limited capturing of temporal dynamics in voltage and current signals, potentially reducing sensitivity to transient islanding events [7]. The paper [8] introduced a novel islanding detection method utilizing Wavelet Transform and artificial neural networks (ANN). While the method demonstrates high accuracy and robustness against noise, the drawback may lie in wavelet selection and computational complexity.

The study conducted in [9] proposed an effective signal processing approach for islanding detection, combining Wiener filtering for signal restoration with Discrete Cosine Transform (DCT) and Discrete Orthogonal Stockwell Transform (DOST) for signal segmentation. While this approach achieves high accuracy, its drawback lies in computational complexity, particularly during the segmentation process, which may lead to increased processing time and resource requirements[9]. Another study [10] presented a passive anti-islanding technique for distributed generation, leveraging the Hilbert–Huang Transform (HHT)

Empirical Mode Decomposition (EMD) decomposes a signal into Intrinsic Mode Functions (IMFs) using a sifting process, enhancing detection performance by isolating oscillatory modes [11]. However, EMD suffers from limitations such as mode mixing and aliasing, where distinct modes are improperly combined or split across IMFs, reducing accuracy.

To address these issues, Ensemble Empirical Mode Decomposition (EEMD) was introduced [12], which reduces mode mixing by adding white noise and averaging the results over multiple noise realizations. While EEMD improves upon traditional EMD, it still suffers from residual noise and mode reconstruction errors, affecting the decomposition quality.

Complete Ensemble Empirical Mode Decomposition with Adaptive Noise (CEEMDAN) was developed to overcome these limitations. CEEMDAN eliminates mode mixing and provides more accurate signal decomposition by adaptively adding white Gaussian noise that fully reconstructs the IMFs without residual noise.

The primary motivation for this study stems from the limitations of existing islanding detection methods and the potential of advanced signal processing techniques and machine learning to address these challenges. The objective is to develop a robust islanding detection method that minimizes the NDZ, ensures high detection accuracy, and operates effectively in real-time scenarios [13].

This study proposes an islanding detection method based on CEEMDAN and a Pattern Recognition Neural Network (PANN). By utilizing CEEMDAN to decompose the negative sequence voltage signal and extracting key features, the method aims to provide precise and reliable islanding detection for grid-connected PV systems

The key contributions of this paper are as follows:

- The proposed method enhanced EMD by leveraging CEEMDAN to extract IMFs from voltage signals, effectively resolving mode mixing and providing more accurate and reliable signal decomposition, leading to higher detection accuracy and faster detection times compared to conventional methods.
- The robustness of the proposed method is validated under various challenging conditions, including power mismatches below 20%, load switching, and fault scenarios, demonstrating its effectiveness across diverse grid disturbances.
- The proposed scheme successfully detects islanding even under zero power mismatch scenarios, significantly reducing the NDZ and thereby enhancing the reliability and safety of distributed generation systems.

II. Materials and Methods

II.1. Non-detection zone (ndz)

The NDZ refers to a specific range or condition wherein an islanding event occurs, but the detection mechanism fails to identify and initiate disconnection from the main grid [14]. This is mainly due to inherent limitations or thresholds within the detection algorithm or mechanism. During the NDZ, the detection system fails to recognize the islanding event, allowing the grid-tied system to continue supplying power to the isolated load, potentially compromising grid stability and safety [15]. The NDZ is specifically identified by its limited mismatch percentage, rendering passive islanding detection methods inefficient within this zone.

The boundaries of the NDZ are established based on predetermined amplitude and frequency values. These values serve as the maximum and minimum allowable limits that the voltage's amplitude and frequency should not surpass. Illustrated in Figure 1, the power flow between the utility grid and the DG source is depicted, highlighting the intricacies of the NDZ.

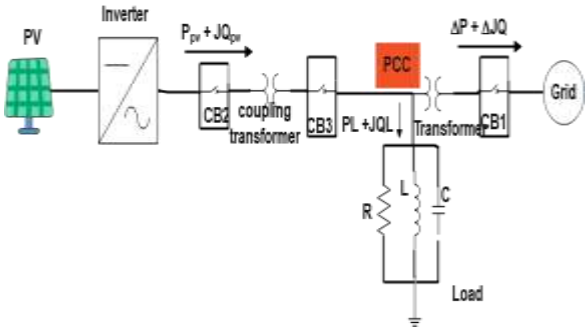

Figure 1. Power flow between the PV-DG and utility grid

The shaded region in Figure 2 signifies the NDZ, which can alternatively be characterized as an area where a power mismatch exists between the utility grid and the DG source. This mismatch is represented using a coordinate system with active power mismatch (ΔP) and reactive power mismatch (ΔQ) axes, as defined in (1) and (2) [16]:

$$\Delta P = P_{DG} - P_{Load} \quad (1)$$

$$\Delta Q = Q_{DG} - Q_{Load} \quad (2)$$

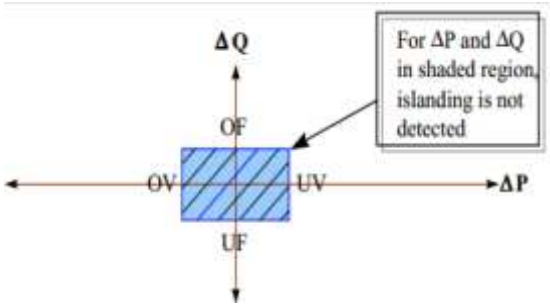

Figure 2. Non-detection Zone (the non-detected area) [16]

P_{DG} and Q_{DG} are the DG source real and reactive power, respectively. Similarly, P_{Load} and Q_{Load} are loads of real and reactive powers, their threshold limits are determined by (3) and (4) [16]

$$\left(\frac{V}{V_{max}}\right)^2 - 1 \leq \frac{\Delta P}{P} \leq \left(\frac{V}{V_{min}}\right)^2 - 1 \quad (3)$$

$$Q\left(1 - \left(\frac{f}{f_{min}}\right)^2\right) \leq \frac{\Delta Q}{P} Q\left(1 - \left(\frac{f}{f_{max}}\right)^2\right) \quad (4)$$

(V_{max}, f_{max}, V_{min} and f_{min}) are the maximum (voltage, frequency) and the minimum (voltage, frequency), respectively, Q is the quality factor, calculated at the PCC, and their values are detected according to the IEEE 1547 series standard are shown in Table 1.

Table 1. Standard IEEE 1547 for anti-islanding techniques [15]

Parameters	Standards
Range of voltage	88% ≤ V ≤ 110%
Range of frequency	49.3 HZ ≤ f ≤ 50.5 HZ
The maximum time of islanding detection	2 sec
Total harmonic distortion (THD%)	≤5%

II.2. Pattern artificial neural network

A PANN is designed to identify patterns and classify data into distinct categories. It is commonly applied in fields such as fault detection [17], diagnostics, load forecasting, and stability control.

The network architecture includes an input layer, one or more hidden layers, and an output layer, as shown in Figure 6. The input layer handles raw data, with the number of neurons matching the number of features in the dataset. Hidden layers transform these inputs using weighted connections and activation functions such as sigmoid, tanh, or ReLU, capturing intricate patterns in the data. The output layer, typically employing a sigmoid activation function for binary classification tasks, produces output values representing the likelihood or confidence level of the data belonging to specific categories.

The PANN is trained to detect patterns and relationships in the data through experience [18]. The neuron, serving as the fundamental unit, processes multiple inputs and applies an activation function. When activated, the neuron transmits its output to other neurons, forming a complex network during the training phase. The activation of neurons can be expressed mathematically using an activation function (f), as demonstrated in (5).

$$Y(t) = f(\sum_{i=1}^{n} x_i(t) w_i(t) + b) \quad (5)$$

Where, t represents the time, b is the bias and, $x_i(t)$, $w_i(t)$, $Y(t)$ represent inputs, neural input weight and output, respectively.

$$sigmoid(x) = \frac{1}{1 + e^{-x}} \quad (6)$$

The PANN is trained using supervised learning techniques, where the network learns from labelled examples. The training process involves adjusting network weights to minimize prediction errors, known as backpropagation [19]. This enables the network to recognize intricate patterns and make accurate predictions.

II.3. CEEMDAN and PANN network-based islanding detection

The methodology section outlines the steps and techniques employed in this study to develop and evaluate the proposed islanding detection method using CEEMDAN and a PANN. The primary focus is on feature extraction, model training, and evaluation metrics. This section is divided into several subsections to provide a detailed explanation of the processes involved.

Complete Ensemble Empirical Mode Decomposition with Adaptive Noise is an advanced signal processing technique that addresses the limitations of traditional EMD and its variant, Ensemble Empirical Mode Decomposition (EEMD). Both EMD and EEMD are widely used for decomposing non-linear and non-stationary signals into a finite set of oscillatory components known as Intrinsic Mode Functions (IMFs). However, EMD suffers from mode mixing, where different oscillatory modes are incorrectly combined within the same IMF, while EEMD introduces noise and residual errors during reconstruction.

CEEMDAN was developed to mitigate these issues by enhancing the decomposition process with adaptive noise. Unlike EEMD, where white noise is added uniformly across all iterations, CEEMDAN adaptively adds white Gaussian noise in each decomposition step to guide the sifting process. This ensures that the IMFs extracted are more precise and freer from mode mixing, while also fully reconstructing the original signal without residual noise. The CEEMDAN method builds upon the strengths of EEMD, further improving the decomposition accuracy and making it more suitable for complex signal analysis.

The process of CEEMDAN is described as follows [20]**:**

1. **Initial Noise Addition:** Add white noise to the original signal:

$$x_i(t) = x(t) + n_i(t) \quad (7)$$

- $x(t)$: Original signal,
- $n_i(t)$ Added white noise for the i-th realization

2. **First IMF Extraction:** Extract the first IMF using EMD from the noisy signal:

$$IMF_{1,i}(t) = EMD(x_i(t))$$

- $IMF_{1,i}(t)$: First IMF from the i-th noisy realization

3. **Ensemble Averaging for First IMF**: Average the first IMF over all noisy realizations

$$IMF_1(t) = \frac{1}{N}\sum_{i=1}^{N} IMF_{1,i}(t) \quad (8)$$

- N: Number of noisy realizations
- $IMF_{1,i}(t)$: First IMF from the i-th realization
- $IMF_1(t)$: Averaged first IMF

4. **Residual Calculation:**

Subtract the averaged first IMF from the original signal to obtain the first residual

$$r_1(t) = x(t) - IMF_1(t) \quad (9)$$

- $r_1(t)$: Residual after extracting the first IMFs
- $x(t)$: Original signal
- $IMF_{1i}(t)$: Averaged first IMF

5. **Adaptive Noise Addition for Subsequent IMFs:** Add adaptive noise to the residual

$$r_{1i}(t) = r_1(t) + n_i(t) \quad (10)$$

- $r_{1i}(t)$: Noisy residual for the i-th realization
- $r_1(t)$: Residual after the first IMF extraction
- $n_i(t)$: Added white noise for the i-th realization

6. **Subsequent IMF Extraction:** Extract the next IMF from the noisy residual:

$$IMF_{2i}(t) = EMD(r_{1i}(t))$$

- $IMF_{2,i}(t)$: second IMF from the i-th noisy realization

7. **Ensemble Averaging for Subsequent IMFs:** Average the second IMF over all noisy realizations

$$IMF_2(t) = \frac{1}{N}\sum_{i=1}^{N} IMF_{2,i}(t) \quad (11)$$

- N: Number of noisy realizations
- $IMF_{2,i}(t)$: Second IMF from the i-th realization
- $IMF_2(t)$: Averaged second IMF

8. **Residual Calculation for subsequent IMFs:** Calculate the residual after subtracting the averaged IMF from the previous residual

$$r_2(t) = r_1(t) - IMF_2(t)$$

$r_2(t)$ is the new residual after subtracting the second IMF

9. Repeat Steps 5-8:

Continue the process iteratively for each IMF until the residual becomes a monotonic function or the maximum number of IMFs is reached.

$$x(t) = \sum_{j=1}^{M} IMF_j(t) + r(t) \quad (12)$$

- $x(t)$: Original signal
- $IMF_j(t)$: j-th intrinsic mode function

M: maximum number of IMFs

Selecting the right IMFs is crucial for accurate feature extraction because not all IMFs contribute equally to the representation of the underlying signal dynamics. To assess the relative importance of different IMFs in representing the underlying dynamics of the signal. The power $\boldsymbol{P_i}$ of the i-th IMF *Ci(t)* is computed using (13). IMF with higher power is considered more significant in representing the underlying dynamics of the signal.

$$\boldsymbol{P_i} = \sum_{\boldsymbol{t=1}}^{\boldsymbol{N}} [\boldsymbol{C_i(t)}]^2 \quad (13)$$

where:

Pi represents the power of the i^{th} IMF.

Ci(t) denotes the ith IMF component at time t

N is the total number of data points.

II.4. Proposed Algorithm for islanding detection

The proposed algorithm, depicted in Figure 3, utilizes negative sequence voltage data at the point of common coupling (PCC) and employs CEEMDAN for preprocessing to extract hidden features. Initially, CEEMDAN decomposes both islanding and non-islanding signals into IMFs. To illustrate this process, an islanding event is triggered at t=1.5 seconds, as shown in Figure 1. The negative sequence voltage signal sampled at the PCC is processed using CEEMDAN, which adapts white Gaussian noise to address mode mixing and extract more distinct IMFs. A one-cycle data window decomposes the signal and extracts the corresponding IMFs. The first IMF captures the highest frequency component of the event, while subsequent IMFs reveal lower frequency components. The energy of each IMF for one cycle is calculated, and significant IMFs are selected based on their 90th-percentile power or energy distribution.

From these significant IMFs, features such as maximum value, standard deviation, and entropy are computed to form a feature vector. This feature vector is used as input to a PANN. The PANN is configured with one input node, neurons in hidden layers, and a single output node. The input vector, comprising the three statistical features from the significant IMFs, is utilized to train the PANN, determining whether islanding occurred.

From the flowchart presented in Figure 3, the proposed method begins with obtaining the negative sequence voltage dataset for both islanding and non-islanding conditions. To enhance the robustness of the decomposition, white Gaussian noise with a standard deviation of 0.6 is introduced to the original signal. CEEMDAN is then applied to these noisy signals to decompose them into IMFs. This process is iterated with the addition of new Gaussian noise across 100 noisy realizations to account for variability and improve the reliability of the decomposition. After completing these iterations, the IMFs obtained from all trials are averaged to produce a final set of IMFs. The significance of each IMF is assessed by evaluating its energy distribution, with IMFs having energy greater than or equal to the 90th percentile considered significant and retained for further analysis. From these significant IMFs, statistical features such as maximum value, standard deviation, and entropy are extracted. These features are used to construct a feature vector for each signal instance. A Pattern Artificial Neural Network (PANN) is then developed and trained using these feature vectors from the training dataset. The trained PANN is employed to classify new instances of negative sequence voltage signals as islanding or non-islanding based on the features derived from the significant IMFs. The methodology concludes with evaluating the islanding detection system's performance to determine the effectiveness and accuracy of the CEEMDAN-based approach.

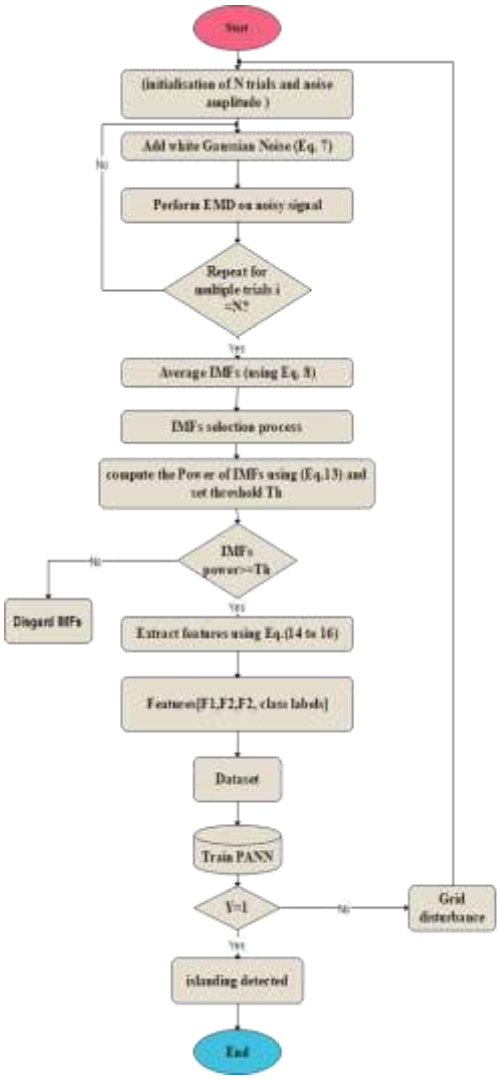

Figure 3. Flowchart for the proposed islanding detection

II.5. Data Generation

To design and assess the proposed islanding detection scheme, a solar photovoltaic (PV) system integrated with a utility grid was modelled and simulated in MATLAB/SIMULINK [21,22]. A negative sequence voltage was recorded at the PCC. Data were sampled at a frequency of 3.84 kHz over a simulation period of 2.5 seconds, ensuring high-resolution measurements to capture the system's dynamic behaviour under varying conditions accurately. From this simulation, two distinct datasets were generated.

The first dataset consists of 294 samples, including islanding and non-islanding conditions. The dataset was generated by decomposing negative sequence voltage to produce IMFs and computing the energy distribution of IMFs to select significant IMFs. The feature vector was designed as a 3 × 294 matrix. This dataset includes 144 islanding cases and 150 non-islanding cases.

The 144 islanding cases covered various scenarios that could lead to islanding.

On the other hand, 150 non-islanding cases were generated, ensuring a diverse set of conditions to train the model robustly.

The second dataset consisted of 64 samples, specifically designed to include challenging conditions that are difficult to discriminate. This dataset is comprised of 16 islanding cases and 48 non-islanding cases. The islanding cases included scenarios where active power and reactive power mismatches varied between -10% and 20%, accounting for zero power mismatch, which is particularly challenging to detect. The 48 non-islanding cases, included load switching up to 100% of the total loading and fault scenarios on different distribution lines by varying the fault location and resistance.

Among the various islanding and non-islanding conditions, zero power mismatch, load switching, and fault scenarios are the most critical to differentiate. Figure 4 illustrates the feature data for these three key conditions. The close proximity of the signals emphasizes the necessity for a robust nonlinear classifier, such as the PANN, to map and distinguish between them accurately.

The different cases generated are listed in Table 2, ensuring a diverse and challenging set of conditions for evaluating the proposed islanding detection method.

Table 2. Description of dataset cases

Case Types	Description	Number of cases
Islanding	Active power mismatch and Reactive power mismatch up to 20%	160
Non islanding	Load switching up to 100%, and fault scenarios	198

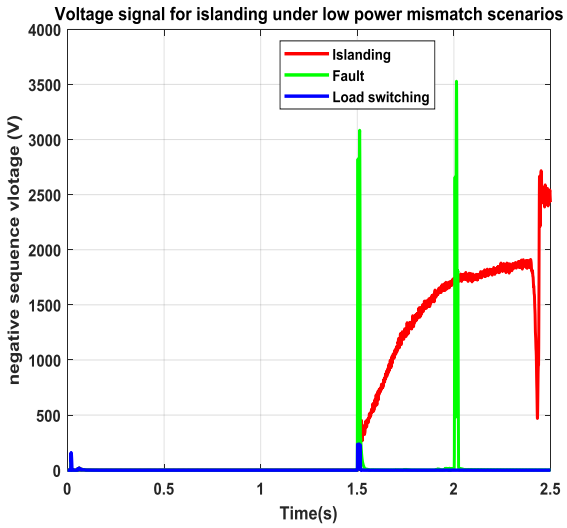

Figure 4. Voltage signal for various islanding scenarios

II.6. Test Case System for Islanding Detection

The single line diagram of the test case system shown in figure 5 was employed to develop and test the proposed method. This test system has been widely used to evaluate and validate many islanding detection methods [21,22]. Developed in MATLAB/Simulink, various scenarios in a power network were simulated as shown in Table 2, providing a controlled environment to generate realistic data for training and testing the islanding detection method.

The test case system was designed to replicate real-world power system conditions, including both normal operational states and various islanding scenarios. Key components of the system include: solar PV distributed generation unit (PV-DG), loads, utility grid, and circuit breakers.

The test system consists of a 2500 MVA, 60 Hz, 120 kV utility grid connected to a distribution network, which includes a 100-kW solar PV system through the PCC.

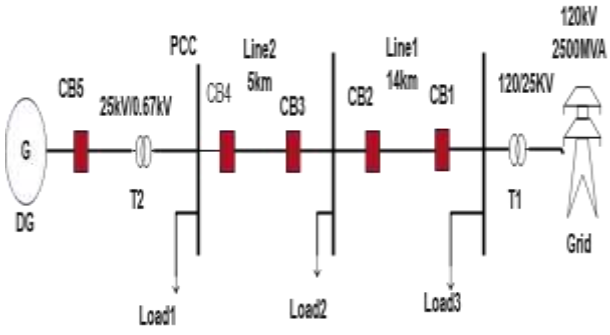

Figure 5. Studied distributed power generation system

II.7. Feature extraction

Three statistical features namely maximum value (max), standard deviation ($\boldsymbol{\mu_i}$), and entropy ($\boldsymbol{\sigma_i}$) were computed from the selected IMFs to form a feature vector using (14), (15) and (16). The features serve as input to the PANN for classification

$$Maximum = max(IMF) \tag{14}$$

Where,

IMF is the intrinsic mode function under consideration

$$standard\ deviation = \sqrt{\frac{1}{N}\sum_{i=1}^{N}(x_i - \bar{x})^2} \tag{15}$$

Where,

x_i are the data points of the IMF.

$\bar{x}$ is the mean of the data points

N is the total number of data points in the IMF.

$$entropy = \sum_{i=1}^{N} p(x_i)\ log_2\big(p(x_i)\big) \tag{16}$$

Where,

$p(x_i)$ is the probability of occurrence of each data point x_i within the IMF

N is the total number of unique data points in the IMF.

II.8. PANN classifier

The structure of the PANN used for islanding detection is depicted with three distinct layers, as shown in Figure 6. Both the input and hidden layers contain 3 neurons each, while the output layer consists of a single neuron. The input layer receives three extracted features (max, $\boldsymbol{\mu_i}$, and $\boldsymbol{\sigma_i}$) as inputs. The output layer produces a binary of 1 to indicate an islanding condition, whereas 0 signifies a non-islanding state.

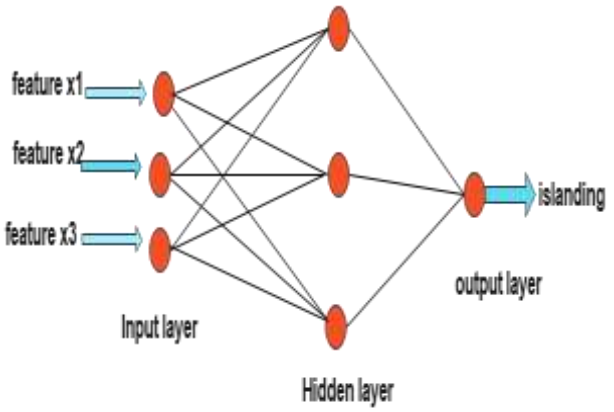

Figure 6. PANN structure with 3 inputs

II.9. Confusion Matrix Analysis

A confusion matrix was created to illustrate the model's classification performance, offering detailed insights into true positives, true negatives, false positives, and false negatives. This analysis provided a comprehensive understanding of the model's strengths and weaknesses in distinguishing between islanding and non-islanding events. For a two-class classifier, the confusion matrix (CM) is represented as follows:

$$CM = \begin{bmatrix} TP & FP \\ FN & TN \end{bmatrix} \quad 17$$

III. Result and discussion

The proposed islanding detection method was evaluated using a variety of techniques and metrics to ensure its robustness and reliability. The evaluation was carried out through confusion matrix analysis, cross-validation, signal feature analysis, and a comparative analysis. The following sections present the results in a logical order, starting with signal feature analysis, followed by confusion matrix analysis, cross-validation performance, and concluding with the comparative analysis.

III.1. Islanding simulation case

Figure 7 illustrates the extracted signal and its IMFs under zero power mismatch conditions. Islanding was initiated at 1.5 seconds. It can be observed that the magnitude of the signal and its corresponding IMFs exhibit minimal variation during the zero-power mismatch condition, making it challenging to differentiate from other grid disturbances. Three IMFs were extracted: IMF1, which contains the highest frequency content and typically carries valuable information; and IMF2 and IMF3, which have progressively lower frequency content. The information captured in these lower frequency IMFs is crucial for accurate islanding detection.

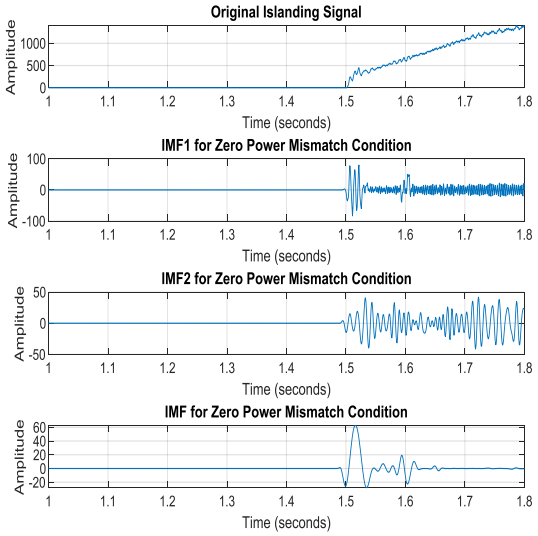

Figure 7. Extracted voltage signal and IMFs

III.2. Islanding Detection Using Signal Features

We examined various signal features based on the analysis of detecting islanding events in a power distribution system. The findings show distinct patterns across islanding and non-islanding scenarios, which provide significant insights into potential detection strategies.

The "Normalized Max Feature," representing the maximum value within the signal, emerged as a key discriminator (see Figure 8). By observing this plot, you can understand how the maximum value of each IMF varies across different IMFs. A higher value indicates a larger maximum amplitude within the IMF. We observed that this feature exhibited notably higher values during islanding events, contrasting with lower values observed during non-islanding instances. This characteristic provides a promising avenue for discriminating between the two scenarios.

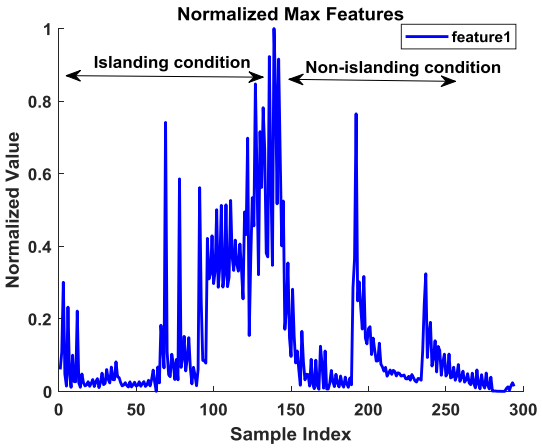

Figure 8. Normalized max feature analysis

Figure 9 shows the analysis of the "Normalized Standard Deviation Feature" unveiled intriguing trends. Specifically, this feature demonstrated larger deviations for islanding scenarios, contrasting with the lower deviations observed during non-islanding conditions. This observation suggests the potential of utilizing standard deviation as a discriminative metric for islanding detection.

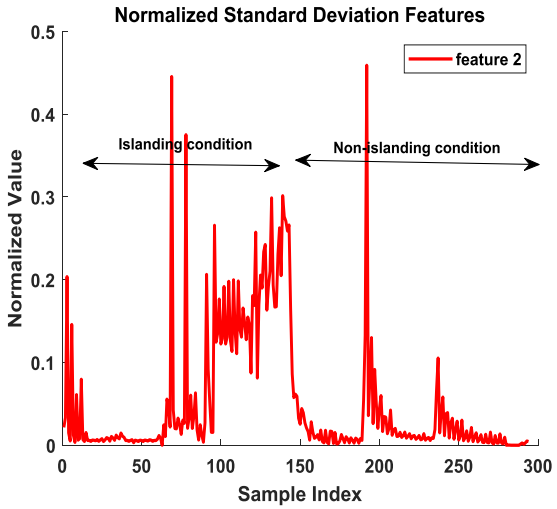

Figure 9. Normalized std features analysis

Figure 10 shows the "Normalized Entropy Feature" emerged as a valuable indicator. Notably, lower entropy values were consistently observed during islanding cases, while higher values were prevalent during non-islanding scenarios. This pattern underscores the utility of entropy as a discriminatory feature for identifying islanding events within the power system.

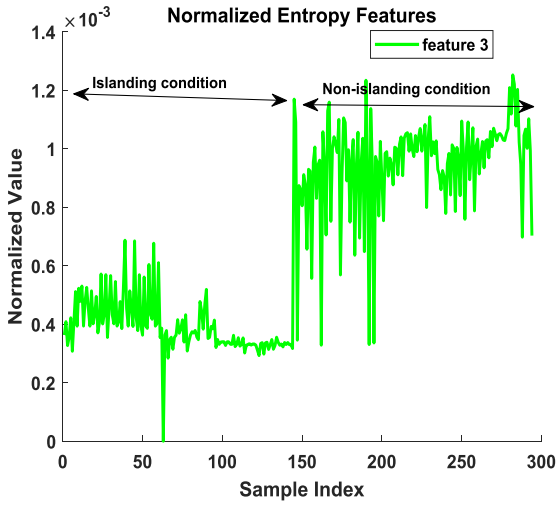

Figure 10. Normalized entropy features analysis

III.3. Confusion Matrix Analysis

The proposed model underwent testing with a power mismatch of less than 20%, yielding significant findings. As depicted in Figure 11, the confusion matrix revealed promising outcomes. Islanding detection achieved a perfect classification rate of 100%, accurately identifying all 16 instances of islanding. Meanwhile, non-islanding detection attained a commendable accuracy of 96%, correctly classifying 46 out of 48 non-islanding cases, with only 2 cases mistakenly identified as islanding.

The detailed performance metrics derived from the confusion matrix are summarized in Table 3.

Table III. PANN Test Results for Power Mismatch

Matrices	Value
accuracy	96.88%
precision	89%
recall	100%
F1 score	94%
Detection time	0.2381 sec

The confusion matrix results indicate that the model is highly effective in detecting islanding events, with a perfect recall (100%) for islanding detection, ensuring that no islanding events are missed. The precision of 89% suggests a high level of confidence in the positive classifications made by the model, with minimal false positives. The overall accuracy of 96.88% and an F1 score of 94% reflect a balanced performance, combining both high precision and recall. The swift detection time of 0.2381 seconds underscores the model's suitability for real-time applications.

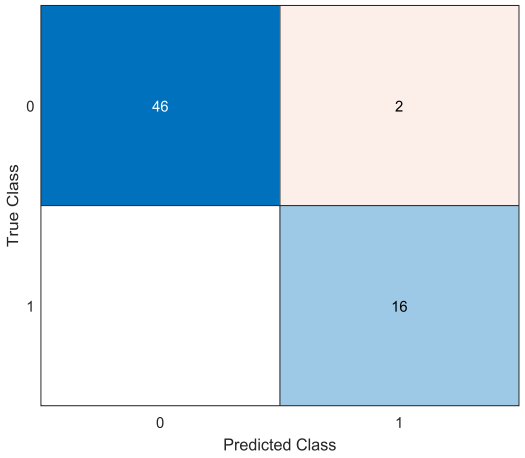

Figure 11. Confusion matrix of the proposed method

- **power mismatch scenarios**

The power mismatch scenarios simulated various islanding conditions, with active power mismatches ranging from -10% to 20% and reactive power mismatches from -5% to 2%. These conditions were meticulously created over specific time indices to test the algorithm's ability to detect islanding events rigorously.

Figure 12 shows the active and reactive power mismatches illustrate the dynamic nature of the simulated scenarios. Active power mismatch exhibited significant fluctuations from -10% to 20% between indices 2 and 7, while reactive power mismatch showed changes from -5% to 2% between indices 1 and 7. These fluctuations represent realistic and challenging conditions under which the detection algorithm was tested. The ability of the algorithm to maintain high performance under these conditions underscores its robustness and reliability.

Achieving NDZ is crucial for ensuring the algorithm can detect islanding conditions without fail, even in the most challenging scenarios. This capability is vital for practical deployment in renewable energy systems, where timely and accurate detection of islanding events can prevent grid disturbances and ensure continuous and reliable power delivery. The study's findings suggest that the developed algorithm not only meets but exceeds these requirements, making it a viable solution for enhancing the stability and reliability of modern power grids.

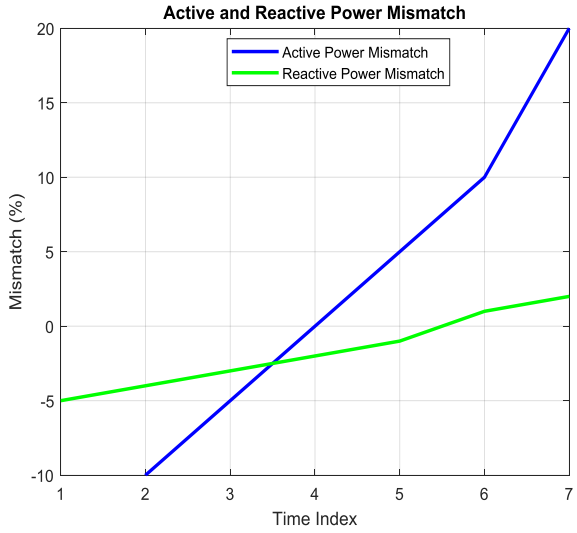

Figure 12. Power mismatch for various islanding conditions

Active power mismatch occurs when the generated active power does not match the load demand and can be either positive or negative. A positive mismatch means more power is generated than consumed, while a negative mismatch means less power is generated than consumed. Similarly, reactive power mismatch happens when the generated reactive power does not meet the reactive power demand. This mismatch can also be positive, where more reactive power is generated than required, or negative, where less reactive power is generated than required.

- **Islanding Detection**

To evaluate the effectiveness of the proposed scheme in identifying critical conditions, the trained PANN model was tested on three unseen cases with a power mismatch below 20%. The corresponding results are shown in Fig. 13. The figure illustrates the voltage waveform and the output trip signal generated by the scheme for the Zero Power Mismatch (ZPM) islanding condition, load switching, and an LLL fault condition, all of which were initiated at t = 1.5 seconds. It is evident that the proposed scheme successfully issued a trip decision during the islanding condition at t = 1.7619 seconds, while no trip signal was triggered for the fault and load switching conditions. Consequently, the detection time can be determined as:

$$\text{Detection time(s)} = \text{trip time} - \text{time occurrence} \quad (8)$$

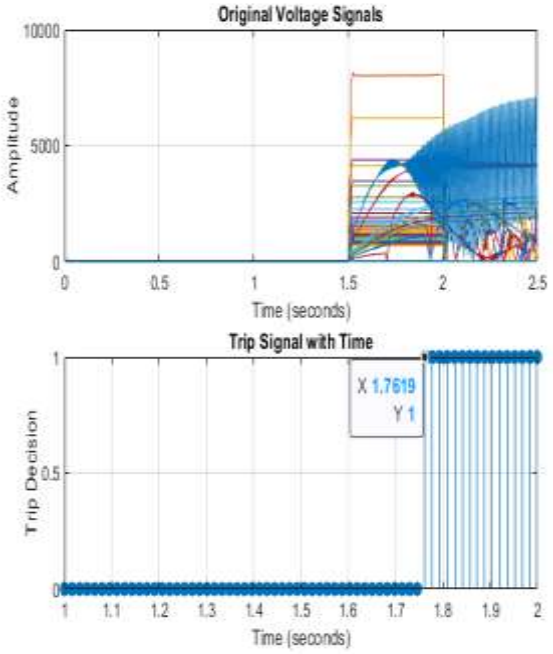

Figure 13. Trip output of the proposed method

III.4. Cross-Validation Performance

To further assess the model's robustness, a 5-fold cross-validation was conducted. This approach helps reduce the risk of overfitting and offers a more generalized evaluation of the model's performance. The cross-validation results are summarized in Table 4.

Table 4. Cross-Validation performance of the proposed islanding detection method

Fold	Accuracy (%)	Precision	Recall	F1_score
1	94.83	0.97	0.93	0.95
2	98.31	1	0.97	0.98
3	94.92	0.97	0.93	0.95
4	96.61	0.97	0.97	0.97
5	98.31	1	0.97	0.98

The cross-validation results show consistently high performance across all folds, with accuracy ranging from 94.83% to 98.31%. Precision values are notably high, ranging from 0.97 to 1, indicating a low rate of false positives. Recall values, ranging from 0.93 to 0.97, ensure that the majority of islanding events are correctly identified. The high F1 scores, ranging from 0.95 to 0.98, demonstrate the model's balanced performance in terms of precision and recall. These results confirm the model's robustness and reliability across different subsets of the data.

III.5. Comparative analysis

The performance of the islanding detection system was evaluated using two methods: Classical EMD and CEEMDAN. The evaluation was conducted based on four key performance metrics: Accuracy, Precision, Recall, and F1-Score. The results are visually represented in Figure 14.

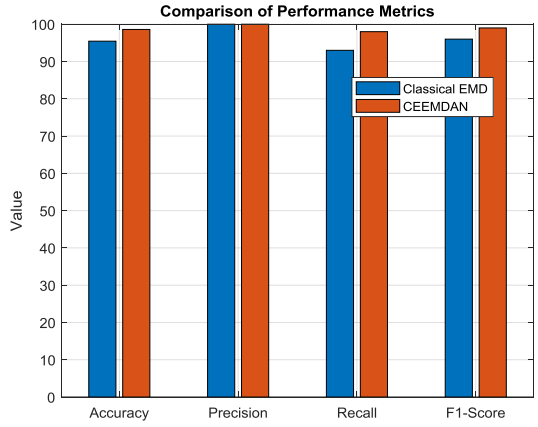

Figure 14. Comparison of performance metrics

The average accuracy achieved using classical EMD is 95.45%. This indicates a high level of effectiveness in distinguishing between islanding and non-islanding events. The proposed CEEMDAN method achieves an even higher accuracy of 98.6%. This improvement suggests that CEEMDAN is more effective in capturing relevant features for classification, leading to more accurate predictions.

The precision for classical EMD is 100%, indicating that all positive predictions (islanding events) made by the model are correct. This shows a very low false-positive rate. Similarly, CEEMDAN also achieves a precision of 100%, matching classical EMD. This consistency demonstrates that both methods are highly reliable in identifying true positives without making incorrect predictions.

The recall for classical EMD is 93%, meaning the model successfully identifies 93% of all actual islanding events. This indicates that some islanding events are missed (false negatives).

CEEMDAN achieves a significantly higher recall of 98%, meaning the method can correctly identify 98% of the actual islanding events. This reflects CEEMDAN's enhanced ability to capture true positives with fewer misses.

The F1-score for classical EMD is 96%, indicating a good balance between precision and recall and reflecting the model's overall effectiveness. CEEMDAN achieves a higher F1-score of 99%, demonstrating its superior balance between precision and recall. This higher F1-score indicates that CEEMDAN is more effective in making accurate and consistent predictions.

The CEEMDAN method shows a clear improvement over classical EMD in terms of accuracy, recall, and F1_score, while maintaining the same high level of precision. These results suggest that CEEMDAN is a more robust and effective method for islanding detection, capturing more relevant features and providing more reliable classification outcomes. Therefore, the enhanced EMD (CEEMDAN) should be considered a superior approach for this application, offering significant benefits in accurately identifying islanding events.

The comprehensive evaluation of the proposed islanding detection method, demonstrates its effectiveness and reliability through signal feature analysis, confusion matrix analysis, cross validation and comparative analysis. The high accuracy, precision, recall, and F1 scores, combined with the swift detection time, indicate that the model is well-suited for real-time islanding detection.

Compared to traditional islanding detection methods, the proposed model significantly improves detection accuracy and speed. Traditional methods often struggle with larger non-detection zones and longer detection times [23],[24] whereas the proposed method achieves a zero non-detection zone and rapid detection, making it a superior solution for enhancing the safety and reliability of grid-connected PV systems.

IV. Conclusion

This paper presents an enhanced islanding detection method for solar PV distributed generation systems based on CEEMDAN and PANN network. The proposed scheme effectively extracts IMFs from voltage signals to identify islanding conditions, achieving high accuracy in the training and testing phases. The model demonstrated a final evaluation accuracy of 98.31% on the full dataset, with an impressive detection time of 0.2381 seconds.

The study conducted extensive simulations to validate the performance of the proposed scheme under various power mismatch scenarios, including critical conditions with mismatches below 20%. Our method consistently issued correct trip decisions for islanding events while avoiding false trips during non-islanding events, such as load switching and fault conditions.

The effectiveness of our scheme in detecting islanding under zero power mismatch (ZPM) conditions demonstrates its robustness and reliability, successfully addressing the challenge of the NDZ. This establishes the proposed method as a promising solution for enhancing the safety and stability of solar PV distributed generation systems. Future work will aim to optimize computational efficiency and explore the application of this method to various types of distributed energy resources and grid configurations.

Declaration

- The authors declare that they have no known financial or non-financial competing interests in any material discussed in this paper.
- The authors declare that this article has not been published before and is not in the process of being published in any other journal.
- The authors confirmed that the paper was free of plagiarism

Reference

[1] A. Serrano-Fontova, J. A. Martinez, P. Casals-Torrens, and R. Bosch, “A robust islanding detection method with zero-non-detection zone for distribution systems with DG,” Int. J. Electr. Power Energy Syst., vol. 133, p. 107247, 2021, doi: 10.1016/j.ijepes.2021.107247.

[2] M. A. Khan, A. Haque, V. S. B. Kurukuru, and M. Saad, “Islanding detection techniques for grid-connected photovoltaic systems-A review,” Renew. Sustain. Energy Rev., vol. 154, no. October 2021, p. 111854, 2022, doi: 10.1016/j.rser.2021.111854.

[3] H. Laaksonen, “Advanced islanding detection functionality for future electricity distribution networks,” IEEE Trans. Power Deliv., vol. 28, no. 4, pp. 2056–2064, 2013, doi: 10.1109/TPWRD.2013.2271317.

[4] A. Al-odienat, “A modified Active Frequency Drift Method for Islanding Detection,” 2021.

[5] L. Xi, Y. Li, Y. Huang, L. Lu, and J. Chen, “A novel automatic generation control method based on the ecological population cooperative control for the islanded smart grid,” Complexity, vol. 2018, 2018, doi: 10.1155/2018/2456963.

[6] D. Velasco, C. L. Trujillo, G. Garcerá, and E. Figueres, “Review of anti-islanding techniques in distributed generators,” Renew. Sustain. Energy Rev., vol. 14, no. 6, pp. 1608–1614, 2010, doi: 10.1016/j.rser.2010.02.011.

[7] A. Ezzat, B. E. Elnaghi, and A. A. Abdelsalam, “Microgrids islanding detection using Fourier transform and machine learning algorithm,” Electr. Power Syst. Res., vol. 196, no. April, 2021, doi: 10.1016/j.epsr.2021.107224.

[8] X. Kong, X. Xu, Z. Yan, S. Chen, H. Yang, and D. Han, “Deep learning hybrid method for islanding detection in distributed generation,” Appl. Energy, vol. 210, no. August 2017, pp. 776–785, 2018, doi: 10.1016/j.apenergy.2017.08.014.

[9] A. V. Soumya and J. Belwin Edward, “Islanding Detection in Microgrid Using Signal Processing Techniques Adopting a Supervised Classifier,” Int. J. Intell. Syst. Appl. Eng., vol. 10, no. 3, pp. 256–264, 2022.

[10] B. K. Chaitanya and A. Yadav, “Hilbert-huang transform based islanding detection scheme for Distributed generation,” 8th IEEE Power India Int. Conf. PIICON 2018, pp. 1–5, 2018, doi: 10.1109/POWERI.2018.8704444.

[11] N. E. Huang et al., “The empirical mode decomposition and the Hubert spectrum for nonlinear and non-stationary time series analysis,” Proc. R. Soc. A Math. Phys. Eng. Sci., vol. 454, no. 1971, pp. 903–995, 1998, doi: 10.1098/rspa.1998.0193.

[12] D. S. Sree.I and Pangedaiah.B, “A New Islanding Detection Technique using Ensemble Empirical Mode Decomposition,” Int. J. Recent Technol. Eng., vol. 9, no. 3, pp. 461–466, 2020, doi: 10.35940/ijrte.c4556.099320.

[13] V. L. Merlin, R. C. Santos, A. P. Grilo, J. C. M. Vieira, D. V. Coury, and M. Oleskovicz, “A new artificial neural network based method for islanding detection of distributed generators,” Int. J. Electr. Power Energy Syst., vol. 75, pp. 139–151, 2016, doi: 10.1016/j.ijepes.2015.08.016.

[14] Y. Li et al., “Nondetection Zone Analytics for Unintentional Islanding in a Distribution Grid Integrated with Distributed Energy Resources,” IEEE Trans. Sustain. Energy, vol. 10, no. 1, pp. 214–225, 2019, doi: 10.1109/TSTE.2018.2830748.

[15] M. Mishra and B. B. Pati, "A hybrid islanding detection method using wavelet transform for hybrid systems with zero non-detection zone," World J. Eng., no. December 2023, 2024, doi: 10.1108/WJE-12-2023-0499.

[16] Y. A. Elshrief, S. Abd-Elhaleem, B. A. Abozalam, and A. D. Asham, "Methods for protecting network from islanding danger," J. Eng. Res., vol. 9, no. 2, pp. 171–183, 2021, doi: 10.36909/jer.v9i2.9695.

[17] M. I. Dieste-Velasco, "Application of a pattern-recognition neural network for detecting analog electronic circuit faults," Mathematics, vol. 9, no. 24, 2021, doi: 10.3390/math9243247.

[18] E. Ceballos Dominguez, M. S. P. Subathra, N. J. Sairamya, and S. Thomas George, "Detection of focal epilepsy in brain maps through a novel pattern recognition technique," Neural Comput. Appl., vol. 32, no. 14, pp. 10143–10157, 2020, doi: 10.1007/s00521-019-04544-8.

[19] A. Thakur, "Fundamentals of Neural Networks," Int. J. Res. Appl. Sci. Eng. Technol., vol. 9, no. VIII, pp. 407–426, 2021, doi: 10.22214/ijraset.2021.37362.

[20] L. Zhao, Z. Li, J. Zhang, and B. Teng, "An Integrated Complete Ensemble Empirical Mode Decomposition with Adaptive Noise to Optimize LSTM for Significant Wave Height Forecasting," J. Mar. Sci. Eng., vol. 11, no. 2, 2023, doi: 10.3390/jmse11020435.

[21] S. Paul, "Islanding Detection in Grid-Connected 100 KW Photovoltaic System Using Wavelet Transform," Int. J. Innov. Res. Sci. Eng. Technol., vol. 5, no. 5, pp. 92–98, 2016.

[22] P. Jaiswal, S. K. Srivastava, and K. B. Sahay, "Modeling and simulation of proposed 100 KW solar PV array power plant for MMMUT Gorakhpur," Int. Conf. Emerg. Trends Electr. Electron. Sustain. Energy Syst. ICETEESES 2016, pp. 261–266, 2016, doi: 10.1109/ICETEESES.2016.7581391.

[23] Z. Guan and Y. Liao, "A New islanding detection method based on wavelet-Transform and ann for micro-grid including inverter assisted distributed generator," Int. J. Emerg. Electr. Power Syst., vol. 20, no. 5, pp. 1–10, 2019, doi: 10.1515/ijeeps-2019-0074.

[24] M. A. Khan, A. Haque, and V. S. B. Kurukuru, "Machine Learning Based Islanding Detection for Grid Connected Photovoltaic System," 2019 Int. Conf. Power Electron. Control Autom. ICPECA 2019 - Proc., vol. 2019-Novem, no. 1, 2019, doi: 10.1109/ICPECA47973.2019.8975614.